**Controls on Geyser Periodicity**

S. E. Ingebritsen; S. A. Rojstaczer

*Science*, New Series, Vol. 262, No. 5135 (Nov. 5, 1993), 889-892.

Stable URL:
http://links.jstor.org/sici?sici=0036-8075%2819931105%293%3A262%3A5135%3C889%3ACOGP%3E2.0.CO%3B2-Q

*Science* is currently published by American Association for the Advancement of Science.

*Trees in Relation to Climate and Solar Activity* (Carnegie Institution of Washington, Washington, DC, 1919); P. M. Brown, M. K. Hughes, C. H. Baisan, T. W. Swetnam, A. C. Caprio, *Tree-Ring Bull.*, in press].
11. R. J. Hartesveldt, *Nat. Hist.* **73**, 12 (1964); N. L. Stephenson, D. J. Parsons, T. W. Swetnam, in *Proceedings—17th Tall Timbers Fire Ecology Conference*, Tallahassee, FL, 18 to 21 May 1989 (Tall Timbers Research Station, Tallahassee, FL, 1991), pp. 321–327; L. Mutch and T. W. Swetnam, in *Proceedings of Symposium on Fire in Wilderness and Park Management, Missoula, Montana*, J. Brown, Tech. Coord., Missoula, MT, 30 March to 1 April 1993 (U.S. Forest Service, Ogden, UT, in press).
12. J. L. Vankat, *Assoc. Am. Geogr. Ann.* **67**, 17 (1977); B. M. Kilgore and D. Taylor, *Ecology* **60**, 129 (1979); H. T. Lewis, "Patterns of Indian Burning in California: Ecology and Ethnohistory," *Ballena Press Anthropol. Pap. No. 1* (Ballena Press, Ramona, CA, 1973).
13. The joint probabilities were the products of the individual probabilities of fire occurrence within each grove, estimated from the observed centennial fire frequencies (annual fire probability equals the number of fires per century divided by 100). This approach is a simplification, because the true fire probabilities were not stationary through time. In addition to the influence of climate change on fire ignition and spread, the accumulation of fuels tends to increase the probability of fire occurrence as a function of time since the last fire. Nevertheless, this test provided a useful measure of how different the observed levels of fire synchrony were among groves, relative to fire synchrony that might have been observed by chance if fire occurrence were random and independent within and among the groves.
14. The observed frequency dependency is not always consistent. Both precipitation and temperature interact to produce droughts and fire responses lasting years to decades. For example, an extreme drought lasting several decades coincided with the largest difference between the regional fire and temperature records during the mid-1200s (Fig. 3). This was one of the driest periods in the tree-ring reconstructions (*6, 8*), and past lake levels in this region also indicate that the mid-1200s were extremely dry [S. Stine, *Palaeogeogr. Palaeoclimatol. Palaeoecol.* **78**, 333 (1990)].
15. R. A. Minnich, *Science* **219**, 1287 (1983). In this case, the shift to lower fire frequency on the U.S. side of the border, and consequent larger chaparral patches and fires, was primarily a result of fire suppression rather than climate.
16. T. W. Swetnam, in "Proceedings of Symposium on Effects of Fire in Management of Southwestern Natural Resources," S. Krammes, Tech. Coord., *Gen. Tech. Rep. RM-191* (U.S. Forest Service, Fort Collins, CO, 1990), pp. 6–17.
17. N. L. Christensen *et al.*, *BioScience* **39**, 678 (1989).
18. R. Abugov, *Ecology* **63**, 2 (1982); T. E. Miller, *Am. Nat.* **120**, 533 (1982).
19. N. L. Christensen, in *Ecosystem Management for Parks and Wilderness*, J. Agee and D. Johnson, Eds. (Univ. of Washington Press, Seattle, 1989), pp. 62–86; N. L. Christensen, *Forum Appl. Res. Public Policy* **4**, 46 (1989).
20. F. H. Bormann and G. E. Likens, *Pattern and Process in a Forested Ecosystem* (Springer-Verlag, New York, 1979).
21. W. H. Romme, *Ecol. Monogr.* **52**, 199 (1982); D. H. Knight, in *Landscape Heterogeneity and Disturbance*, M. G. Turner, Ed. (Springer-Verlag, New York, 1987), pp. 59–83.
22. I thank the many assistants, students, National Park Service personnel, California Department of Forestry personnel, and volunteers who contributed by carrying out field, shop, and laboratory tasks, foremost among whom were C. H. Baisan, P. M. Brown, A. C. Caprio, and R. Touchan of the Laboratory of Tree-Ring Research, University of Arizona; I also thank J. L. Betancourt, L. J. Graumlich, M. K. Hughes, D. J. Parsons, N. L. Stephenson, and two anonymous reviewers for commenting on and editing the manuscript. Supported by Sequoia, Kings Canyon, and Yosemite National Parks and National Park Service Global Change Program Cooperative Agreements, Department of the Interior 8018-1-0002 and 8032-1-0002.

11 June 1993; accepted 30 August 1993

# Controls on Geyser Periodicity

S. E. Ingebritsen* and S. A. Rojstaczer

**Geyser eruption frequency is not constant over time and has been shown to vary with small ($\leq 10^{-6}$) strains induced by seismic events, atmospheric loading, and Earth tides. The geyser system is approximated as a permeable conduit of intensely fractured rock surrounded by a less permeable rock matrix. Numerical simulation of this conceptual model yields a set of parameters that controls geyser existence and periodicity. Much of the responsiveness to remote seismicity and other small strains in the Earth can be explained in terms of variations in permeability and lateral recharge rates.**

In contrast to steady surface-discharge features such as fumaroles and hot springs, which are common in regions with active geothermal systems, periodic geysers are rare (*1*). Most occur in areas where the water table is near the land surface and hydrostatic boiling-point conditions are present to depths of about 200 m. Geyser systems are commonly described in terms of a shallow low-permeability seal (*1*) or constriction (*2*) underlaid by a chamber that periodically erupts a steam-water mixture (*1–3*) (Fig. 1A). In this model, eruption magnitude and frequency are governed by chamber and seal geometry.

To examine geyser periodicity in a quantitative fashion, we invoke a modification of the chamber model. We approximate the chamber as a zone of fractured rock (Fig. 1B). Instead of being constricted only at the top of the chamber, flow is controlled everywhere in the fracture zone by fracture permeability. The fluid-saturated fracture zone is a permeable, compliant column surrounded by less permeable and less compliant rock. We determined a set of parameters that controls geyser periodicity by numerical simulation of the fracture-zone model.

Geyser eruption frequency is not constant over time (*4*). For most geysers, eruption frequency is irregular, especially when other geysers exist nearby (*5*). Even famously regular geysers such as Old Faithful of Yellowstone exhibit variations in their eruption intervals (*6*). Over various time scales, eruption interval has been shown to vary with small strains (typically less than 1 μ-strain) induced by variations in atmospheric loading, Earth tides, and seismic events (*4, 7–8*). Much of this responsiveness to small strains should be controlled by changes in model parameters.

We investigate geyser behavior using a mathematical model of heat and mass transport in permeable media. The flow of fluid and heat is described by coupled, multiphase mass- and energy-balance equations (*9*)

$$\partial (n\rho_f)/\partial t - \nabla \cdot [\bar{\bar{k}} k_{rs}\rho_s/\mu_s \cdot (\nabla P - \rho_s g \nabla D)] - \nabla \cdot [\bar{\bar{k}} k_{rw}\rho_w/\mu_w \cdot (\nabla P - \rho_w g \nabla D)] - q_m = 0 \quad (1)$$

and

$$\partial/\partial t[n\rho_f h_f + (1-n)\rho_r h_r] - \nabla \cdot [\bar{\bar{k}} k_{rs}\rho_s h_s/\mu_s \cdot (\nabla P - \rho_s g \nabla D)] - \nabla \cdot [\bar{\bar{k}} k_{rw}\rho_w h_w/\mu_w \cdot (\nabla P - \rho_w g \nabla D)] - \nabla \cdot [K_m(\partial T/\partial P)_h \nabla P + K_m (\partial T/\partial h)_p \nabla h] - q_h = 0 \quad (2)$$

respectively, where $D$ is depth, $g$ is gravitational acceleration, $h$ is enthalpy, $\bar{\bar{k}}$ is the

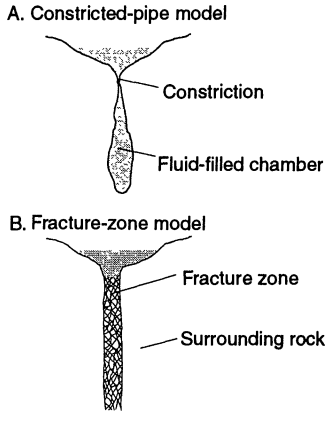


**Fig. 1.** (**A**) Commonly cited model of geyser geometry and (**B**) fracture-zone model. In (B), characteristics for the fracture zone include high permeability and high compressibility, whereas the surrounding rock exhibits low permeability and low compressibility.

S. E. Ingebritsen, U.S. Geological Survey, Menlo Park, CA 94025.
S. A. Rojstaczer, Department of Geology, Duke University, Durham, NC 27708.
*To whom correspondence should be addressed.

intrinsic permeability tensor, $K_m$ is the thermal conductivity of the saturated medium, $k_{rs}$ and $k_{rw}$ are the relative permeabilities to steam and liquid water, respectively, and depend on volumetric liquid saturation $S$ [$0 \leq k_r(S) \leq 1$], $n$ is porosity, $P$ is pressure, $T$ is temperature, $t$ is time, $\rho$ is density, $\mu$ is dynamic viscosity, and $q_m$ and $q_h$ are mass and energy source and sink terms, respectively. The subscript $f$ designates the fluid mixture in place [$\rho_f = S\rho_w + (1 - S)\rho_s$], $r$ refers to the porous medium (rock), $s$ refers to steam, $w$ refers to liquid water, and *sat* refers to saturated conditions. These coupled equations are solved numerically, with constitutive relations that describe $h_{w,sat}(P_{sat})$, $h_s(P_{sat})$, $T(P, h_w)$, $\rho_w(P, h_w)$, $\rho_s(P, h_s)$, $\mu_w(T)$, and $\mu_s(T)$ (*10*).

This model conserves mass and energy and allows countercurrent and cocurrent flow of steam and liquid water at variable rates. It does not account for capillary pressure differences between phases and assumes that fluid and rock are in thermal equilibrium (*11*). With respect to the geyser problem, a more important limitation is the assumption of Darcian (linear laminar) flow. This assumption is probably appropriate for parts of the geyser cycle and possibly for conditions at depth throughout the cycle. However, near-vent flow rates during geyser eruptions are such that much energy is dissipated by turbulence. For turbulent conditions, our simulations overestimate the flow rates associated with a particular hydraulic gradient.

We simulated the subsurface geyser system as a deep fracture zone surrounded by a less permeable matrix (Fig. 2). The lower boundary of the geyser conduit has a constant heat flux or steam flux, and the upper boundary of the system is set to a constant pressure and enthalpy. Pressures and enthalpies at the edges of our two-dimensional model slice are maintained at the hydrostatic boiling point, and the faces of the slice are treated as closed and insulated. In most simulations there was no mass flux at the lower boundary of the system, so the upper and lateral boundaries were the sources of mass recharge. The representation of the upper boundary is most appropriate for geysers that erupt through pools with near-constant depths.

The initial conditions for all simulations involved boiling-point temperatures corresponding to the hydrostatic pressure at a given depth. Parameters that were varied in the course of our numerical simulations included the permeability, porosity, and dimensions of the fracture zone; the permeability contrast between fracture zone and matrix; basal heat input at the lower boundary (*12*); and the temperature and pressure at the upper boundary.

The geyser simulations achieved a fairly constant eruption interval (±10%) within

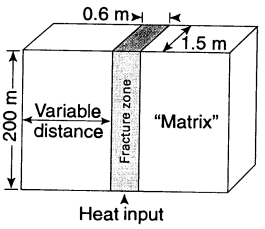


**Fig. 2.** Two-dimensional model of a geyser conduit as a fracture zone embedded in a lower permeability rock matrix. See Figs. 3, 5, and 6 for other parameters.

two to three eruption cycles. Two representative geyser cycles for a laterally isolated fracture zone are shown in Fig. 3. Before an eruption, the fracture zone is almost entirely liquid-saturated (Fig. 4). Where steam is present, it flows upward relatively rapidly, and upflow and condensation of steam transfer substantial amounts of heat toward the surface. During an eruption, the volume changes associated with the conversion of liquid water to steam drive liquid up through the fracture zone. The eruption is shallow-rooted in the sense that most mass discharge is obtained from the upper part of the fracture zone; in this example, roughly two-thirds of the mass is from depths of <40 m. The relative contribution from any depth range can be calculated by comparison of the pre-eruption and post-eruption saturation curves (Fig. 4).

For the parameters shown in Fig. 3, the eruption interval is about 21 min and maximum discharge rates are about 50 kg $s^{-1}$ (Fig. 3A). At mid-eruption the geyser conduit is filled with a two-phase mixture (Fig. 4). Mid-eruption discharge at the exit plane is only about 6% steam by mass (Fig. 3A) but 99% steam by volume, because of the 1600-fold density difference between the phases at 100°C and about 1 bar pressure. Liquid discharge ceases when the pressure gradient in the upper part of the geyser conduit drops below the hydrostatic state, but minor steam discharge continues (Fig. 3A) as long as a steam phase is present in the upper part of the conduit (Figs. 3B and 4). As long as the pressure gradient remains subhydrostatic, the fracture zone receives mass recharge. Before the next eruption, it is again nearly liquid-saturated (Fig. 4) (*13, 14*). The simulated discharge is periodic rather than steady because the loss of mass and energy during an eruption is faster than the recharge rates. For the isolated fracture zone of Figs. 3 and 4 there is no mass recharge during an eruption, because the upper boundary is the only source of mass.

We next examined the influence of lateral recharge to the fracture zone by varying the permeability contrast between the fracture zone and matrix (Fig. 5). For a permeability contrast of $\geq 10^4$ between fracture

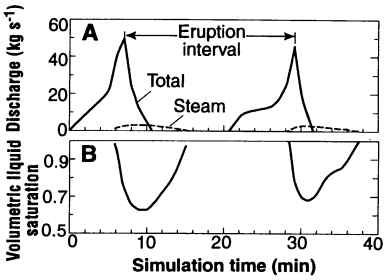


**Fig. 3.** (**A**) Mass discharge and (**B**) volumetric liquid saturation at the exit plane for a simulation of an isolated fracture zone with the following parameters: permeability, $10^{-8}$ $m^2$; porosity, 0.75; thermal conductivity, 2 W $m^{-1}$ $K^{-1}$; and basal heat input, 2.5 MW. We assume the following relations for the relative permeabilities to liquid water ($k_{rw}$) and steam ($k_{rs}$) as functions of liquid saturation ($S$): $k_{rw} = (S - 0.3)/0.7$, and $k_{rs} = 1 - k_{rw}$. The fracture-zone geometry is shown in Fig. 2.

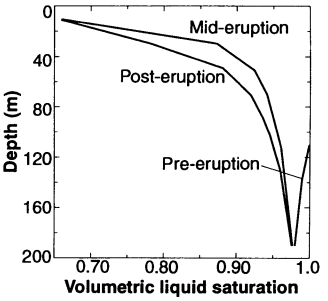


**Fig. 4.** Volumetric liquid saturation within the fracture zone at selected times during the geyser cycles shown in Fig. 3.

zone and matrix (Fig. 5A), the eruption frequency (20 min) and magnitude were constant and nearly identical to those shown for the isolated fracture zone in Fig. 3. For a permeability contrast of $10^3$, the eruption interval was reduced by about 15%. A further, small decrease in the permeability contrast extinguished the periodic behavior of the system (Fig. 5A) and led to weak (about 0.1 kg $s^{-1}$), steady discharge from the fracture zone. Analogous results were obtained when matrix permeability was held constant and distance to the lateral boundaries was decreased (Fig. 5B). The eruption interval stayed fairly constant until periodic behavior disappeared over a narrow distance range. These results indicate that geyser behavior is particularly sensitive to lateral recharge of the fracture zone. Geyser conduits that are recharged by lateral flow are probably $10^3$ to $10^4$ times as permeable as the surrounding rock. Smaller permeability contrasts lead to steady hot-spring discharge, and unless much of the erupted fluid is recycled, larger permeability contrasts would lead to higher enthalpy, fumarole-like discharge.

Under conditions in which the fracture

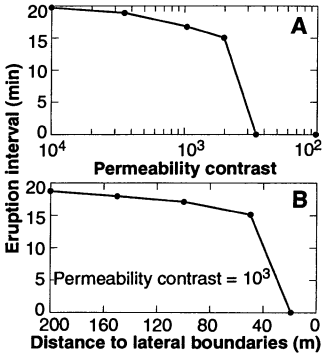


**Fig. 5.** Interval between geyser eruptions as a function of (**A**) permeability contrast between the fracture zone ($10^{-8}$ m$^2$) and the adjacent rock matrix, with lateral boundaries at distances of 100 m, and (**B**) distance to the lateral boundaries, with a permeability contrast of $10^3$ (fracture zone, $10^{-8}$ m$^2$; matrix, $10^{-11}$ m$^2$). Basal heat input is 0.5 MW, and the values of other parameters are as shown in Figs. 2 and 3.

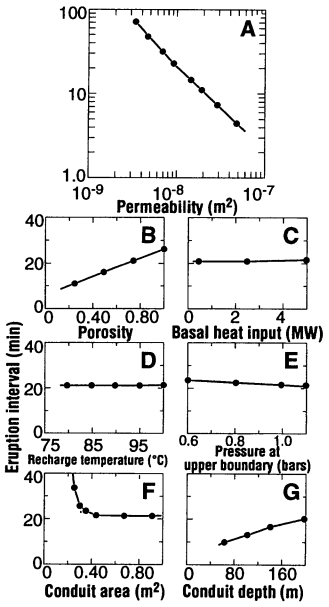


**Fig. 6.** Interval between geyser eruptions from a laterally isolated fracture zone as a function of (**A**) fracture-zone permeability, (**B**) fracture-zone porosity, (**C**) heat input at the base of the fracture zone, (**D**) temperature and (**E**) pressure at the upper boundary, (**F**) fracture-zone area, and (**G**) fracture-zone depth. Other parameters are as shown in Figs. 2 and 3.

zone was completely isolated from the surrounding matrix, fracture-zone permeability exerted the strongest control on geyser behavior, with eruption frequency scaling with permeability (Fig. 6A). Increasing the permeability from $0.35 \times 10^{-8}$ to $5.0 \times 10^{-8}$ m$^2$ reduced the eruption interval from 70 to 4 min (*15*). Porosity (Fig. 6B) also influenced eruption frequency; varying the porosity from 0.01 to 1.0 increased the eruption interval from 6 to 27 min. The sensitivity to permeability and porosity of the fracture zone can also be interpreted as a recharge effect; decreasing permeability and increasing porosity both retard migration of the recharge front and thus favor less frequent, larger eruptions.

In contrast to the sensitivity of eruption frequency to permeability and porosity, alterations in the basal heat input and temperature of the recharging fluid had little effect (Fig. 6, C and D). However, varying basal heat input between 0.0025 and 5.0 MW did cause maximum mass discharge rates to vary from ~0.5 to 80 kg s$^{-1}$ and time-averaged heat discharge to vary from ~0.005 to 10 MW, a range that encompasses most natural hot springs and geysers. Varying the temperature of the recharging fluid also caused changes in eruption magnitude.

Fracture-zone geometry can exert a strong influence on eruption frequency and magnitude (Fig. 6, F and G). For a small enough conduit area, intermittent liquid-dominated discharge gives way to steadier, steam-dominated flow, interspersed with shorter recharge intervals. This transition takes place because, given a constant basal heat input, the enthalpy of the discharge must increase as conduit area is reduced. The eruption interval and magnitude increase with conduit depth; although discharge is dominated by water that originates at shallow depths (Fig. 4), heat transfer from greater depths is an important part of the geyser cycle (*16*).

We now consider the responsiveness of geysers to small strains in light of the simulation results. The strains induced by atmospheric loading, Earth tides, and remote seismicity ($\leq 10^{-6}$) translate to small porosity changes. It follows that elastic response to such strains is unlikely to cause significant changes in fracture permeability or in the permeability of an open conduit (*17*). As an alternative, we invoke fluid-pressure changes to explain geyser response to cyclic loading and ground-motion effects to explain the response to remote seismicity.

The influence of recharge rate (Fig. 5) may help to explain why small strains induced by atmospheric loading can sometimes influence eruptive behavior. If the geyser conduit is more compliant than the surrounding matrix, pore fluids in the conduit likely pressurize more than pore fluids in the surrounding rock in response to increases in atmospheric loading (*18*). This differential response causes a net reduction in lateral recharge to the geyser conduit. The eruption frequency can be expected to be inversely correlated with atmospheric pressure (*4*) if lateral flow is a significant component of the recharge cycle (*19*).

Strains by Earth tides could also induce changes in lateral recharge (*18*). Associated changes in pore-fluid pressures in this case are less in the relatively compliant geyser conduit than in the surrounding rock, increasing the potential for recharge (*18*). Thus, peak tidal compression may be positively related to eruption frequency.

The influence of atmospheric loading or Earth tides should be subtle in most cases. Associated fluid-pressure changes are generally <0.02 bar, equivalent to a change in water level of about 0.2 m. For the uniform fracture zone shown in Fig. 2, a 0.2-m change in water level translates to a fluid contribution of <200 kg, or <2% of the mass discharged during one of the eruptions shown in Figs. 3 and 4. The influence of cyclic loading should be more significant for geysers with smaller time-averaged discharge rates and could be amplified if water levels in the geyser conduit varied within a relatively large "chamber."

The simulation results may also suggest why geyser behavior can be modified by seismicity. Both increases and decreases in eruption magnitude and frequency have been observed (*7–8*). Increases in frequency may be caused by ground-motion–induced permeability increases in the fracture zone (Fig. 6A) or in the surrounding matrix (Fig. 5A) (*20*). Our simulations suggest that permeability increases in the fracture zone would lead to roughly proportional increases in frequency (Fig. 6A). However, if ground motion is sufficient to reopen sealed fractures at depth and the fracture zone is lengthened, eruption frequency may decline (Fig. 6G). Significant declines would seem to indicate large changes in effective conduit length. Because the dynamic and static shear strains caused by distant earthquakes are small (*21*), such lengthening might be related to the reopening of a network of preexisting fractures rather than the creation of new fractures.

Changes in eruptive behavior induced by seismicity are not permanent. Even in the absence of seismicity, geysers evolve over time. Our results indicate that the geyser process can take place in fracture zones that have a much higher permeability than the surrounding rock and that geyser periodicity is highly sensitive to changes in hydraulic properties. Thus relatively gradual processes such as silica deposition also change geyser behavior. The existence and character of a geyser depends on a unique set of physical conditions that should not be long-lived.

## REFERENCES AND NOTES

1. D. E. White, *Am. J. Sci.* **265**, 641 (1967).
2. S. W. Kieffer, *Rev. Geophys.* **27**, 1 (1989).
3. R. O. Fournier, *Science* **163**, 304 (1969).
4. J. S. Rinehart, *J. Geophys. Res.* **77**, 342 (1972); G. D. Marler and D. E. White, *ibid.*, p. 5825; J. S. Rinehart, *ibid.*, p. 5830.
5. G. D. Marler, *Am. J. Sci.* **249**, 329 (1951).
6. J. S. Rinehart, *Science* **150**, 494 (1965).
7. P. G. Silver and N. J. Valette-Silver, *ibid.* **257**, 1363 (1992).
8. R. A. Hutchinson, *U. S. Geol. Surv. Open-File Rep.*

85-290 (1985), p. 612; J. S. Rinehart, *Geysers and Geothermal Energy* (Springer-Verlag, New York, 1980). Seismicity can also create geysers [G. D. Marler and D. E. White, *Geol. Soc. Am. Bull.* **86**, 749 (1975)].
9. C. R. Faust and J. W. Mercer, *Water Resour. Res.* **15**, 23 (1979).
10. ———, *ibid.*, p. 31. We used a revised version of the Faust and Mercer algorithm for heat and mass transport provided by D. O. Hayba (written communication).
11. It would be difficult to determine an appropriate capillary-pressure function for this system; relevant data are limited. The assumption of fluid-rock thermal equilibrium has a minor effect on our simulations. For the simulation depicted in Figs. 3 and 4, cyclic temperature variations range from ~2°C at 190 m in depth to ~10°C at 10 m in depth. About $7 \times 10^5$ kJ per cycle is exchanged with the rock (relative to a throughflow rate of $\sim 7 \times 10^6$ kJ per cycle). Models that explicitly calculate fluid-rock heat exchange would tend to predict lesser values, depending on the assumed fracture spacing.
12. The injection of pure heat over much of the range of simulated rates (0.0025 to 5.0 MW per 0.9 $m^2$) seems physically implausible; focused steam upflow and condensation are a more likely heat-input mechanism. The geyser cycles shown in Figs. 3 and 4 involved the injection of 2.5 MW, which could be supplied by <1 kg $s^{-1}$ (0.893 kg $s^{-1}$) of steam at 215°C (2800 kJ $kg^{-1}$). Nearly identical geyser cycles were obtained when saturated steam was injected at the base of the column. Basal heat input rates as low as 0.0025 MW, corresponding to <0.001 kg $s^{-1}$ of steam injection, were sufficient to induce periodic behavior (Fig. 6C), albeit with drastically reduced eruption magnitudes.
13. For the simulations in Figs. 2 and 3, the mass discharge is about 11,000 kg per eruption, or 30,000 kg per hour, similar to that estimated for Old Faithful, Yellowstone (24,000 kg per hour; R. A. Hutchinson, oral communication). The time-averaged heat discharge is 5.5 MW, also similar to the Old Faithful rate, calculated on the basis of an estimated steady recharge rate of 6 kg $s^{-1}$ (*2*) from a liquid reservoir at 215°C (*14*). The simulated heat discharge is much larger than the heat input at the base of the fracture zone (2.5 MW) because about 3.0 MW is obtained from recharge water at 100°C.
14. R. O. Fournier, *Annu. Rev. Earth Planet. Sci.* **17**, 13 (1989).
15. The period is also affected by the choice of relative permeability functions. Compared to the linear functions used here, "fracture-flow" functions increase eruption frequency and Corey-type functions decrease frequency. The fracture-flow functions assume that relative permeability to steam increases rapidly as liquid saturation decreases [M. L. Sorey, M. A. Grant, E. Bradford, *Water Resour. Res.* **16**, 767 (1980)], whereas with Corey-type functions steam is relatively immobile at moderate to high liquid saturations [A. T. Corey, *Soil Sci. Soc. Proc.* **21**, 7 (1957)].
16. There is field evidence for a deep root to some geyser activity. Enthalpy-chloride and enthalpy-silica relations indicate that the water discharged from Old Faithful, Yellowstone, has boiled adiabatically from temperatures >200°C (equivalent to depths of ≥180 m) (*14*). Further, instruments placed in a geysering geothermal well in Guatemala indicated that boiling occurs to depths of at least 800 m during geyser-like discharge periods [D. E. Michels, *Proc. Workshop Geotherm. Reservoir Engl.* **16**, 255 (1991)].
17. Under unusual conditions, it is conceivable that the permeability of the surrounding matrix would be affected. For example, if essentially all recharge to the geyser conduit occurs through thin (2-mm), subhorizontal, widely spaced (50-m) fractures, and a vertical strain of $10^{-6}$ is wholly accommodated by this fracture set, the fracture permeability of the matrix ($\sim 10^{-11}$ $m^2$) will vary by ~10%.
18. S. A. Rojstaczer and D. C. Agnew, *J. Geophys. Res.* **94**, 12403 (1989).
19. We ignored atmospheric loading effects and tested whether geyser periodicity was influenced by the magnitude of atmospheric pressure at the land surface. We varied atmospheric pressure between 0.6 and 1.0 bar, holding other parameters constant, and found no significant change in eruption frequency (Fig. 6E).
20. Permeability increases associated with seismicity have been documented in the region near the Loma Prieta earthquake (10/17/89, **M** 7.1) [S. A. Rojstaczer and S. C. Wolf, *Geology* **20**, 211 (1992)]. Silver and Valette-Silver (*7*) proposed that the response of Calistoga "Old Faithful" to Loma Prieta and other remote earthquakes is due to changes in permeability or pore volume in the rock matrix adjacent to the geyser conduit.
21. D. P. Hill *et al.*, *Science* **260**, 1617 (1993).
22. We thank J. D. Bredehoeft, R. O. Fournier, P. A. Hsieh, and two anonymous referees for helpful reviews of earlier versions of the manuscript, and D. R. Jones for drafting the figures.

27 July 1993; accepted 3 September 1993

# Formation of a Molten Globule Intermediate Early in the Kinetic Folding Pathway of Apomyoglobin

Patricia A. Jennings and Peter E. Wright*

**Hydrogen exchange pulse labeling and stopped-flow circular dichroism were used to establish that the structure of the earliest detectable intermediate formed during refolding of apomyoglobin corresponds closely to that of a previously characterized equilibrium molten globule. This compact, cooperatively folded intermediate was formed in less than 5 milliseconds and contained stable, hydrogen-bonded secondary structure localized in the A, G, and H helices and part of the B helix. The remainder of the B helix folded on a much slower time scale, followed by the C and E helices and the CD loop. The data indicate that a molten globule intermediate was formed on the kinetic folding pathway.**

Molten globules have been postulated as universal folding intermediates formed on the kinetic folding pathways of all proteins (*1*). The term "molten globule" describes a partially folded state with a molecular volume intermediate to that of the native and the unfolded states, a relatively high content of secondary structure, and few fixed tertiary interactions (*1–3*). Two-dimensional (2D) NMR studies of these intermediate species (*4–6*) have been used to establish the presence of elements of hydrogen bonded secondary structure in which amide protons are protected from exchange. Although equilibrium molten globules have been detected for a few proteins under appropriate conditions of pH, temperature, and ionic strength (*2, 3, 7–9*), it has been unclear whether this species actually participates in kinetic folding events.

Apomyoglobin (apoMb) (Fig. 1) is one of the few proteins studied that forms an equilibrium molten globule. The molten globule state is populated at low pH and temperature (*8, 10, 11*), is compact, and contains substantial secondary structure (~35% helix) that appears to be largely associated with folding of the A, G, and H helices (*4*). To investigate the kinetic folding pathway(s) and the role of the molten globule in folding, we have undertaken stopped-flow circular dichroism (CD) and hydrogen exchange pulse-labeling studies of the apoMb refolding reaction.

ApoMb is well suited for studies of folding mechanisms. The absence of the heme group makes folding unimolecular, the protein is stable under various conditions, and the NMR spectrum of the carbon-monoxy complex of the holoprotein has been assigned (*12*). Although the structure of apoMb has not been determined, all available data (*4, 10, 13, 14*) indicate that it has a compact hydrophobic core that resembles the tertiary structure of the holoprotein. The differences between the apo and holoproteins appear to be largely confined to the F helix region, which abuts the heme and provides the proximal histidine ligand (*4, 14*).

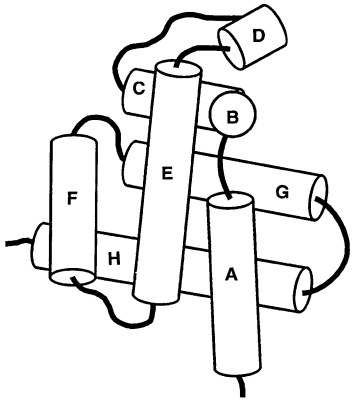


**Fig. 1.** Scheme of Mb with the eight α helices (A to H) indicated.

Department of Molecular Biology, The Scripps Research Institute, 10666 North Torrey Pines Road, La Jolla, California 92037.

*To whom correspondence should be addressed.